Molecular Origins of Selectivity in the Reduction of NO_x by NH_3

Donghai Sun,[†] William F. Schneider,*[,‡] James B. Adams,[†] and Debasis Sengupta[§]

Department of Chemical and Materials Engineering, Arizona State University, Tempe, Arizona 85287, Physical and Environmental Sciences Department, Ford Motor Company, Mail Drop 3083/SRL, Dearborn, Michigan 48121-2053, and CFD Research Corporation, 215 Wynn Drive, Huntsville, Alabama 35805

Received: March 1, 2004; In Final Form: August 10, 2004

The fundamental principle underlying the selective catalytic reduction (SCR) of NO_x to N_2 is the promotion of reactions of reductant with NO_x over competing, and thermodynamically preferred, reactions with a large excess of O_2. A similar competition between NO_x and O_2 exists in the noncatalytic, thermal reduction of NO_x with NH_3. In this work, density functional theory calculations are used to elucidate the origins of the remarkable selectivity in thermal deNO_x. Thermal deNO_x is initiated by the conversion of NH_3 into the active reductant, NH_2 radical. NH_2 radical reacts with NO at rates typical of gas-phase radical reactions to produce a relatively strongly bound H_2NNO adduct that readily rearranges and decomposes to N_2 and H_2O. In contrast, NH_2 radical reacts exceedingly slowly with O_2: the H_2N-OO adduct is weakly bound and more readily falls apart than reacts to products. The pronounced discrimination of NH_2 against reaction with O_2 is unusual behavior for a radical but can be understood through comparison of the electronic structures of the H_2NNO and H_2NOO radical adducts. These two key elements of thermal deNO_x—reductant activation and kinetic inhibition of reactions with O_2—are similarly essential to successful catalytic lean NO_x reduction, and are important to consider in evaluating and modeling NO_x SCR.

Introduction

NO_x, including nitric oxide (NO) and nitrogen dioxide (NO_2), is a key precursor in the formation of tropospheric ozone and acid rain, and thus NO_x removal from combustion sources remains a high priority for environmental protection.[1−4] Highly effective NO_x conversion to N_2 can be achieved with "three-way catalysts"[4,5] as are now nearly universally applied for automotive exhaust after-treatment. The effectiveness of these catalysts is limited to exhaust from stoichiometric combustion, which contains only small amounts of interfering O_2. Effective catalysis for NO_x control in the presence of a large excess of O_2, as arises from diesel, lean-burn gasoline, and many types of stationary combustion sources, remains an outstanding challenge.

One method for "lean" NO_x control from stationary sources is the thermal deNO_x process, by which NO_x is selectively and noncatalytically reduced to N_2 with NH_3 reductant.[6−9] NH_3 (or urea as an NH_3 precursor) is injected directly into an exhaust gas stream where it homogeneously titrates NO_x. The thermal deNO_x process can be described by the following net reactions: [6,7]

$$4NO + 4NH_3 + O_2 \rightarrow 4N_2 + 6H_2O \quad (1)$$

$$2NO + 4NH_3 + 2O_2 \rightarrow 3N_2 + 6H_2O \quad (2)$$

NO conversion to N_2 competes with NH_3 oxidation, with the result that useful conversion is found only in a relatively narrow temperature window around 1200 K.[8,9] A key observation is that thermal deNO_x consumes O_2 as part of the reduction chemistry.

In the selective catalytic reduction (SCR) of NO_x with NH_3, base metal oxide catalysts are used to increase NO_x conversion efficiency and to lower the temperature range of maximum conversion.[2,10] The precise stoichiometry varies with reaction conditions and catalysts, but the overall chemistry in general follows the pattern of reactions 1 and 2. In both the thermal deNO_x and SCR processes, the NH_3 reductant exhibits high selectivity for NO_x over O_2 despite the much higher concentration of O_2 (typically several orders of magnitude greater than the NO_x concentration) and the large inherent thermodynamic preference for consumption of reductant by O_2. Reactions 1 and 2 must compete with NH_3 oxidation, either to N_2 (the thermodynamically preferred product)

$$4NH_3 + 3O_2 \rightarrow 2N_2 + 6H_2O \quad (3)$$

or to NO (the kinetically preferred product)

$$4NH_3 + 5O_2 \rightarrow 4NO + 6H_2O \quad (4)$$

The thermal deNO_x process relies on the inherent preference for NH_3 to react with NO_x over O_2; in SCR, the catalyst must maintain or enhance this selectivity. While the thermal and catalytic chemistries likely differ in detail, an understanding of the origins of selectivity in the thermal system should shed light on the much less well-understood chemistry underlying selective catalysis.

In thermal deNO_x chemistry, the amino (NH_2) radical is the reductant that reacts directly with NO to ultimately produce N_2. These NH_2 radicals are generated in chain reactions that involve O atoms and OH radicals, and as a consequence O_2 is a necessary ingredient in the thermal deNO_x process.[8,11] Competition between NO and O_2 for the "activated" NH_2 reductant is thus inherent to the overall chemistry. The reactions of NH_2 with NO and O_2 have been studied extensively both

* To whom correspondence should be addressed. E-mail: wschnei2@ford.com. Telephone: (313) 323-2064. Fax: (313) 322-7044.
[†] Arizona State University.
[‡] Ford Motor Company.
[§] CFD Research Corporation.

10.1021/jp049079a CCC: $27.50
Published on Web 09/30/2004

theoretically and experimentally:[10−48]

$$NH_2 + NO \rightarrow \text{Products} \quad (5)$$

$$NH_2 + O_2 \rightarrow \text{Products} \quad (6)$$

Fortunately for the practical application, reaction 5 is observed to be many orders of magnitude faster than reaction 6. Reaction 5 has a negative apparent activation energy (or negative temperature dependence) overall, with second-order rate constant decreasing from 10^{-11} at room temperature to 10^{-12} cm^3 molecule^{-1} s^{-1} at 2000 K.[12,23,24,35,36,44] At the low-temperature end, this rate is within an order of magnitude of the gas kinetic collision limit. In contrast, the most recent estimates of the rate constant for reaction 6 are on the order of 10^{-21} cm^3 molecule^{-1} s^{-1} at room temperature,[12,27,31,32,45,46] or 10 orders of magnitude less than reaction 5. This large difference for these seemingly similar reactions can be contrasted with the rate constants for reactions 7 and 8:[48]

$$CH_3 + NO \rightarrow \text{Products} \quad (7)$$

$$CH_3 + O_2 \rightarrow \text{Products} \quad (8)$$

Reaction 7 is isoelectronic with reaction 5 and at room temperature has a comparable rate constant of approximately 10^{-11} cm^3 molecule^{-1} s^{-1}. Reaction 8 is isoelectronic with reaction 6 yet has a rate constant of 10^{-12} cm^3 molecule^{-1} s^{-1}, or 9 orders of magnitude greater than that of 6. The distinctly lower rate of reaction 6 compared to reaction 8 persists to higher temperature, and is clearly an anomaly with rather fortuitous consequences.

Despite their distinctly different rates, reactions 5 and 6 proceed through topologically similar microscopic reaction channels. The primary and key secondary channels of reaction 5 are[8,12,15−18,21,38]

$$NH_2 + NO \rightarrow N_2 + H_2O \quad (9)$$

$$\rightarrow HN_2 + OH \quad (10)$$

$$\rightarrow N_2O + H_2 \quad (11)$$

The last of these is observed to be unimportant under conditions relevant to thermal deNO_x, while channel 10 is a minor but crucial channel because it is chain branching:[8,44] further reactions of the HN_2 and OH radical products generate two NH_2 radicals for every one consumed. Channel 9[49] is exothermic in the gas phase by −125 kcal mol^{-1} while channel 10 is approximately thermoneutral.[18] The branching ratio of channels 10 to 9 is a key parameter controlling thermal deNO_x and increases from approximately 0.1 at room temperature to 0.5 at 1600 K.[34,44] The reaction 6 analogues to channels 9 and 10 are the following:

$$NH_2 + O_2 \rightarrow NO + H_2O \quad (12)$$

$$\rightarrow HNO + OH \quad (13)$$

and are exothermic by −82 and −12 kcal mol^{-1}, respectively.[49] In addition, a third, endothermic channel may compete with these[12,19]

$$NH_2 + O_2 \rightarrow H_2NO + O \quad (14)$$

All of these reactions of NH_2 with NO and O_2 are both known to begin with reactant association and to proceed by internal H rearrangements to yield products.

Although reactions 5 and 6 have been studied separately in detail, there has been less attention paid to understanding the molecular origins of the very different kinetics of these superficially similar reactions. In this paper, we provide the first complete, side-by-side comparison of the potential energy surfaces of these two reactions using a consistent level of density functional theory (DFT). We find, consistent with earlier analysis,[12] that the key discriminator between the two is the much greater stability of the initial H_2NNO adduct relative to H_2NOO radical, and that after this first association step, the potential energy surfaces for the two reactions are remarkably similar. We show that this binding energy difference can be understood through comparison of the computed electronic structures of H_2NNO and H_2NOO radical, and this comparison allows us to rationalize kinetic trends in other R + NO vs R + O_2 reactions. Further, we use these results to infer mechanistic requirements for NO_x selective catalytic reduction, in particular illustrating that inhibition of reactions of reductant with O_2 is as critical as promotion of reactions with NO for effective catalysis.

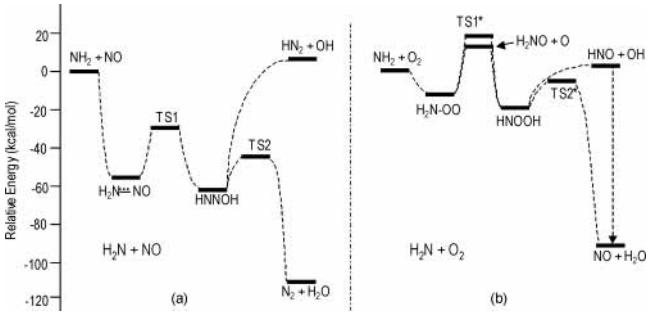

Figure 1. BLYP-calculated potential energy surfaces for reactions (a) NH2 + NO and (b) NH2 + O2. HNXOH (X = N, O) isomerization details hidden for clarity.

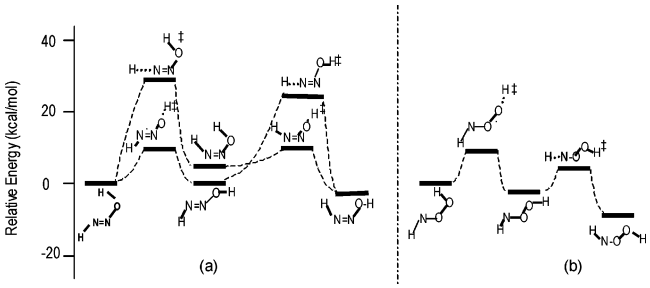

Figure 2. BLYP-calculated potential energy surfaces for isomerization of (a) HNNOH and (b) HNOOH.

Computational Method

DFT calculations were performed with the Amsterdam Density Functional (ADF) package.[50] Molecular structures, vibrational frequencies, and energies were determined within the spin-polarized BLYP approximation.[51−53] A valence double-ζ plus polarization Slater-type basis was used on all atoms. Integration parameters were chosen to ensure that numerically evaluated integrals were accurate to five significant digits. With these integration mesh parameters, total energies are converged to < 0.1 kcal mol^{-1} and geometries are converged to < 0.001 Å. Vibrational frequencies were calculated by two-sided numerical differentiation of analytical energy gradients and were used with standard statistical mechanical formulas to calculate 298 K enthalpies. The optimized and transition state structures are characterized by zero and one imaginary vibrational frequency.

Results

Figures 1 and 2 summarize the key potential energy surface results for reactions 5 and 6, and details of the calculated structures are included in Figures 3, 5, 6, and 7. Tables 1 and

TABLE 1: Comparison of BLYP-Computed Reaction Energies with Previously Reported Values for $NH_2 + NO$ Reaction Steps (Energies in kcal mol^{-1})

reaction step	BLYP	B3LYP[18]	PMP4[18]	CCSD(T)[18]	G2M(CCI)[18]	GVB-CI[55]	BAC-MP4[57]	MP4SDQ[17]	CASSCF/ SCF-CI[33]	CASSCF/ ICCI[16]
$NH_2 + NO \rightarrow H_2NNO$	−53.5	−44.3	−38.2	−39.1	−47.0	−29.1	−48.4	−37.5	−35.1	−44.0
$H_2NNO \rightarrow$ *trans,cis*-HNNOH	1.8	1.5	1.1	−1.2	0	−2.0	1.0	1.0	−2.0	−2.1
trans,cis-HNNOH → *cis,cis*-HNNOH	1.1	1.0	1.9	2.0	0.9	1.1	2.2	2.0	1.1	1.2
trans, cis-HNNOH → *trans, trans*-HNNOH	4.7	6.0	6.0	7.0	5.9	8.1	6.2	6.8	6.8	
cis,cis-HNNOH → *cis,trans*-HNNOH	−2.1	−1.0	−2.1	−1.0	0	−1.3	−1.9	−2.0	0	0
trans, trans-HNNOH → *cis, trans*-HNNOH	−5.7	−6.1	−6.0	−7.0	−6.1	−9.2	−6.3	−7.2	−5.8	
cis, trans-HNNOH → $N_2 + H_2O$	−69.8	−72.2	−80.2	−79.1	−78.0	−91.8	−77.0	−77.1	−84.0	−79.0
$NH_2 + NO \rightarrow N_2 + H_2O$	−125.4	−115.0	−118.0	−117.7	−123.9	−124.0	−124.3	−113.0	−120.2	−124.1

TABLE 2: Comparison of BLYP-Computed Energy Barriers with Previously Reported Values for $NH_2 + NO$ Reaction Steps (Energies in kcal mol^{-1})

reaction step	BLYP	B3LYP[18]	PMP4[18]	CCSD(T)[18]	G2M(CCI)[18]	BAC-MP4[57]	MP4SDQ[17]	CASSCF/ SCF-CI[33]	CASSCF/ ICCI[16]
$H_2NNO \rightarrow$ *trans,cis*-HNNOH	30.0	31.8	30.0	31.1	32.3	28.0	34.5	35.0	30.1
trans, cis-HNNOH → *cis,cis*-HNNOH	10.4	9.8	10.1	10.0	9.2		10.3	9.0	10.1
trans, cis-HNNOH → *trans,trans*-HNNOH	31.4	35.7	41.1	42.1	39.0		43.8	41.8	
cis, cis-HNNOH → *cis, trans*-HNNOH	27.8	32.4	37.2	38.2	36.1	39.2	41.0	39.2	37.1
trans, trans-HNNOH → *cis,trans*-HNNOH	3.8	4.1	4.1	3.0	3.5		1.1	3.1	
cis, trans-HNNOH → $N_2 + H_2O$	20.4	22.8	21.0	24.3	21.2	22.1	28.4	26.3	24.0

TABLE 3: Comparison of BLYP-Computed Reaction Energies with Previously Reported values for $NH_2 + O_2$ Reaction Steps (Energies in kcal mol^{-1})

reaction step	BLYP	B3LYP[19]	MP2[19]	QCISD[19]
$NH_2 + O_2 \rightarrow H_2NO_2$	−14.7	−2.8	5.8	−0.2
$H_2NO_2 \rightarrow H_2NO + O$	25.2	32.6	24.6	27.3
$H_2NO_2 \rightarrow HNOOH$	4.1	0.7	−2.3	0.1
$HNOOH \rightarrow NO + H_2O$	−65.4		−84.8	−75.4
$NH_2 + O_2 \rightarrow H_2O + NO$	−81.5		−80.3	−75.5

TABLE 4: Comparison of BLYP-Computed Energy Barriers with Previously Reported Values for $NH_2 + O_2$ Reaction Steps (Energies in kcal mol^{-1})

reaction step	BLYP	B3LYP[19]	MP2[19]	QCISD[19]
$NH_2 + O_2 \rightarrow H_2NO_2$	no barrier	5.8	6.2	7.9
$H_2NO_2 \rightarrow HNOOH$ (I)	29.4	33.5	29	33.6
HNOOH (I) → HNOOH (II)	1.2			
HNOOH (II) → HNOOH (III)	2.0			
HNOOH (III) → $NO + H_2O$	5.2			

3 compare computed BLYP energetics with other reported theoretical results for both reactions. A similar comparison for activation energies is shown in Tables 3 and 4. In general, BLYP-calculated reaction enthalpies corrected to 298 K and 1.0 atm agree well with experimental data for both reactions.[54] The reported results are also in good agreement with previous literature values for geometries (not shown for brevity). The energetics are generally in good qualitative and semiquantiative agreement with the range of previous theoretical values, and the BLYP calculations provide a good basis for drawing qualitative comparisons between the two reaction potential energy surfaces. Significant differences are the following. (1) For $NH_2 + NO$, the first step has a somewhat larger reaction enthalpy, and the last step has a somewhat smaller reaction enthalpy. However, the net reaction enthalpy agrees well with other theoretical and experimental data. (2) For $NH_2 + O_2$, the first step is somewhat more negative than other reports, but the last step is somewhat more positive. The net reaction enthalpy agrees well with other theoretical and experimental results. In the following we consider in more detail analogous reaction steps for both reactions.

H_2N-XO (X = N, O) Adduct Formation. Both reactions 5 and 6 begin with reactant association to form H_2NXO adducts, where X = N and O for the NO and O_2 reactions, respectively. The structure of the H_2NNO adduct is shown in Figure 3 and compares well with that reported previously.[22] The adduct is closed-shell and planar, with N−N (1.35 Å) and N−O (1.24 Å) bond lengths both characteristic of partial double bonds. The short N−N separation is consistent with the formation of a strong H_2N-NO bond. The BLYP-calculated bond energy is −54 kcal mol^{-1}, somewhat higher than that calculated using explicit electron correlation methods.[22]

The origins of the strong H_2N-NO bond can be understood by reference to the qualitative molecular orbital diagram in Figure 4a. (One should note that, for simplicity and clarity, bonds that are distributed among several canonical orbitals, such as the N−N σ bond, are idealized as belonging to a single orbital.) The chemistry of the NO radical is dominated by the singly occupied 2π orbitals, which are polarized toward the N center and which make NO both a good electron donor and acceptor. The NH_2 radical has an occupied in-plane (σ-) orbital that overlaps well with the in-plane component of the NO 2π system to form the σ component of the N−N bond. This interaction is further enhanced by hybridization with the NO 5σ level (and to a lesser extent by the in-plane 1π orbitals, not shown in Figure 4 for simplicity) to yield the low-lying N−N bonding level, the nonbonding, O-centered orbital that is the highest occupied orbital, and the high-lying, unoccupied N−N antibonding level. Complementing the σ system are N−N π bonding and antibonding orbitals formed from overlap of the unhybridized NH_2 2p level and the out-of-plane component of the NO 2π system. Double occupation of the bonding orbital produces a net N=N double bond. Again, this π system is modified by interactions with the NO 1π orbitals, but the qualitative picture is unchanged. The π bonding accounts for the planarity of H_2NNO and imposes a large barrier to rotation about the N−N bond. Bonding results in a net charge transfer of 0.23 electrons from the NH_2 to the NO fragment, as measured by Mulliken population analysis, consistent with the dative σ/covalent π bonding picture.

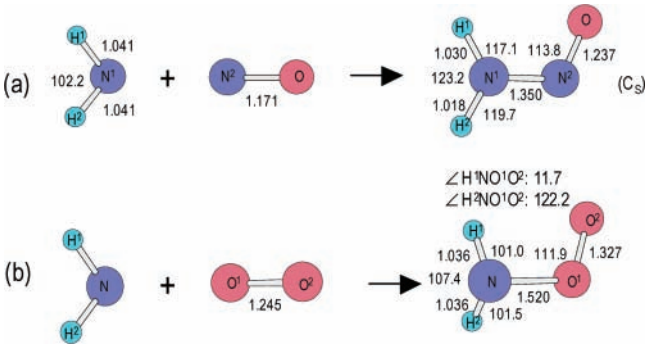

Figure 3. BLYP-calculated structures of (a) H_2NNO and (b) H_2NOO radical adducts.

The strong H_2N-NO bond stands in sharp contrast to the H_2N-OO bond in the aminoperoxyl radical formed from the association of NH_2 and O_2. As shown in Figure 3, the BLYP-optimized H_2NOO radical is nonplanar, with an N−O bond length (1.41 Å) comparable to a typical N−O single bond (1.40 Å)[56] and O−O bond length only slightly perturbed from that of molecular O_2.[19] These structural features reflect the absence of π bonding between the NH_2 and O_2 fragments, and suggest that even the σ bond between the two is weak. The BLYP-calculated association energy is −15 kcal mol^{-1}, again slightly overestimating the QCISD-calculated bond strength.[19]

The O_2 molecule readily combines with many radicals so it is interesting that the H_2N-OO bond is so weak. O_2 has one more electron than NO; if the H_2NOO radical retained the planar structure of H_2NNO, this additional electron would reside in the strongly antibonding N−N π^* orbital second from the top in the molecular orbital scheme shown in Figure 4a. To reduce this unfavorable interaction, the H_2NOO radical relaxes to a nonplanar conformation in which rotation about the N−O bond is essentially unhindered. Figure 4b shows a schematic molecular orbital diagram for the nonplanar H_2NOO radical in one C_s conformation. The H_2NNO π bond clearly separates into an N-centered lone pair and a singly occupied O−O π^* state that is destabilized by unfavorable nonbonded interactions with the NH_2 fragment. The impact on the σ manifold is subtler, but poor orbital overlap between the N-centered σ orbital and the O_2 2π state further contribute to the weak bonding. As with H_2NNO, the net direction of charge transfer is from the NH_2 to the O_2 fragment in forming the weak σ bond; as suggested by the MO diagram, essentially all the unpaired electron spin density is localized on the O_2 fragment.

Within the BLYP approximation, formation of both H_2NXO adducts proceeds without activation barrier, and more sophisticated electronic structure calculations support this conclusion for the more exothermic $H_2N + NO$ reaction.[18] Gradient-corrected DFT methods are well-known to underestimate energy

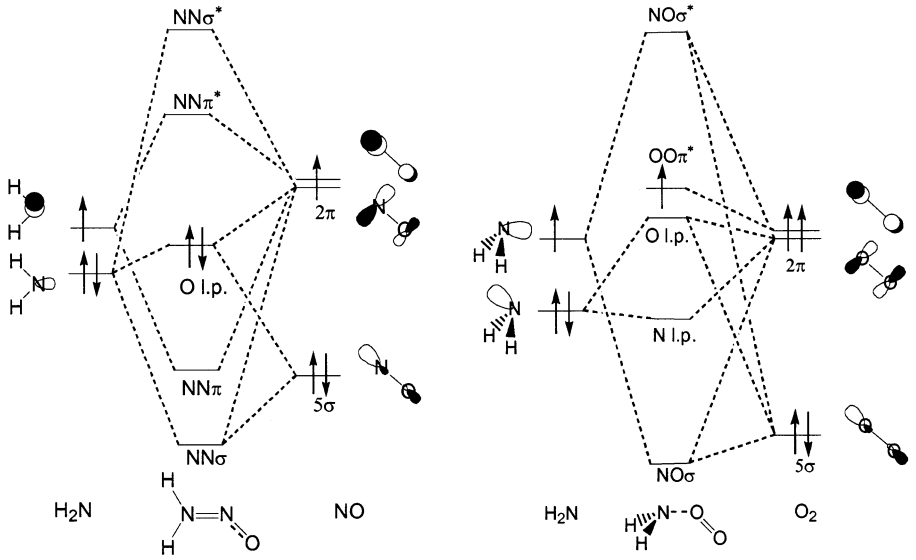

Figure 4. Schematic molecular orbital diagrams of (a) H_2NNO and (b) H_2NOO radical.

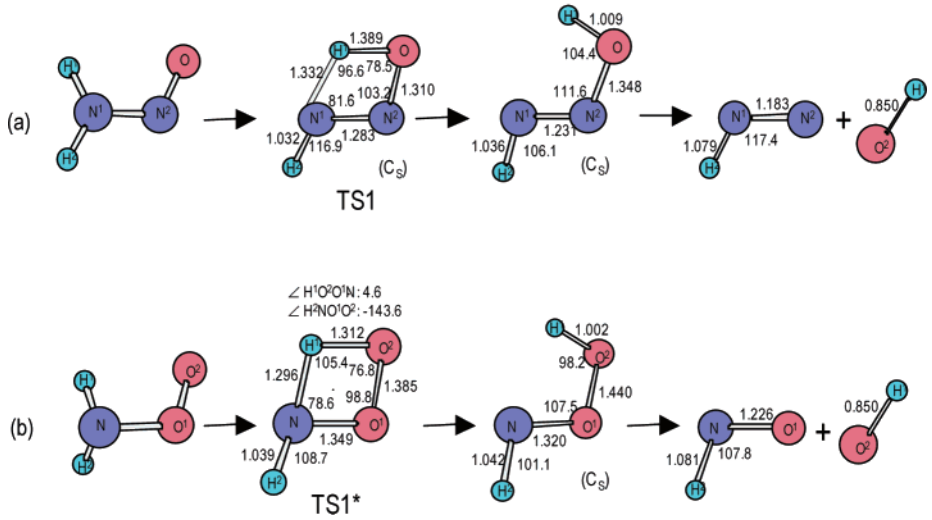

Figure 5. BLYP-calculated structures along (a) $H_2NNO \rightarrow HNNOH$ and (b) $H_2NOO \rightarrow HNOOH$ pathways.

barriers, and in fact more sophisticated hybrid DFT,[19] QCISD,[19] and empirically corrected MP4 calculations[57] all predict a small barrier to association of NH_2 radical and O_2 (Table 4).

$H_2NXO \rightarrow H_2NX + O$ (X = N, O) Decomposition. Once formed, the H_2NXO adducts face three possible fates: decomposition back to reactants, direct reaction to products, and internal H rearrangements leading to products. The only significant direct reaction pathway for H_2NOO radical is O atom loss

$$H_2NOO \rightarrow H_2NO + O \qquad (15)$$

Reaction 15 is calculated to be 25 kcal mol^{-1} endothermic (see Figure 1), comparable to that reported previously.[18] This exit channel is slightly higher in energy than the $H_2N + O_2$ reactants and thus is a minor competitor to decomposition to reactants. In contrast, the comparable H_2NNO reaction to H_2NN and O is highly endothermic (124 kcal mol^{-1}) and of no importance. As seen in Figure 4a, N−O π^* states are depleted in H_2NNO, leading to a shortening and strengthening of the N−O bond.

H_2NXO (X = N, O) → HNXOH 1,3 H-Transfer. Adduct rearrangement and reaction begins with 1,3 H-transfer, in each case breaking one N−H and creating one O−H bond. This similarity is more than superficial: the energetics (Figure 1) and structural modifications (Figure 5) along the two reaction paths are quite similar. Both H-transfer reactions are slightly exothermic and proceed with comparable barriers through four-membered-ring transition states. The calculated energy barriers with respect to adducts are both 30 kcal mol^{-1}, in good agreement with previous theoretical evaluations of 28−34 kcal mol^{-1} for the H_2NNO[16−18,22] and 31−34 kcal mol^{-1} for H_2NOO radical.[19] H-transfer is accompanied by shortening of the N−X and lengthening of the X−O bonds. From H_2NNO to HNNOH the N−N bond length decreases from 1.35 to 1.23 Å, a value typical of an N═N double bond (1.25 Å),[56] while the N−O bond lengthens from 1.24 to 1.35 Å. Some amount of π bonding is retained in the N−O bond, as the HNNOH molecule is planar, and as discussed below, rotations about the N−N and N−O bonds produce four unique conformations. Similarly, along the path from H_2NOO radical to HNOOH the N−O bond length decreases from 1.52 to 1.32 Å and the O−O bond increases from 1.33 to 1.44 Å, again ending in a planar product with partial double bond character within the N−O−O backbone. The four-electron π system in HNNOH is isoelectronic with that in the well-known allyl anion ($C_3H_5^-$); planar HNOOH has a five-electron π system that exhibits substantial conformational variability, as discussed below.

HNX−OH (X = N, O) Homolytic Cleavage. Channels 10 and 13 are completed by homolytic cleavage of the HNN−OH and

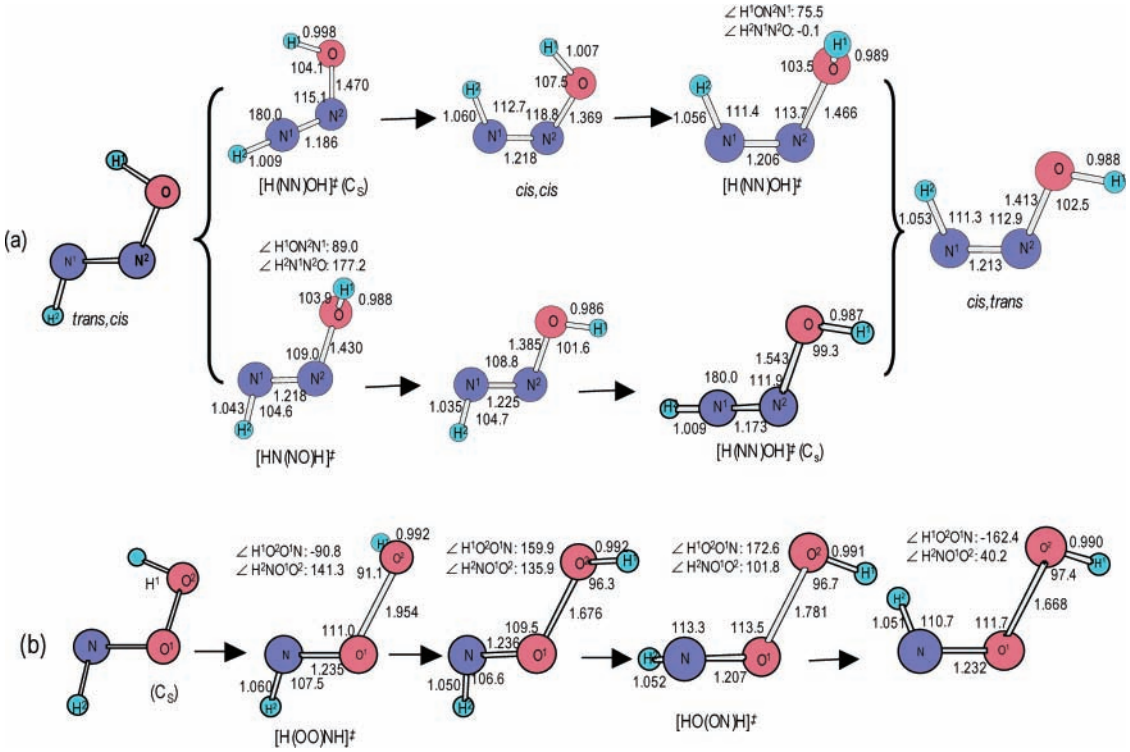

Figure 6. BLYP-calculated structures for isomerization of (a) HNNOH and (b) HNOOH radical.

HNO−OH bonds, as shown in Figure 1. Both reactions yield metastable products slightly higher in energy than the NH_2 + XO entrance channels. The former cleavage reaction is highly endothermic and proceeds without barrier to HN_2 and OH products. The existence of this minor channel is crucial for thermal deNO_x chemistry, as HN_2 radical readily decomposes to N_2 and an H atom; two radicals (H and OH) are thus generated that can ultimately convert NH_3 molecules into reaction-sustaining NH_2 radicals.[8] The HNO−OH bond is long and weak, and cleavage occurs with small activation barrier to HNO and OH radical products.

HNXOH (X = N, O) Conformational Isomerization. Competing with the homolytic cleavage channels is formation of the energy minimizing reaction products NX and H_2O via a second 1,3 H-transfer step. Preceding this step, the HNXOH must rotate into a conformation that places the transferring H atom in proximity with the O center. Figure 2 shows the calculated potential energy surfaces for HNXOH conformational isomerization, and Figure 6 shows the structural details of these processes.

HNNOH exhibits double bond character about both N−N and N−O bonds, and as a result can exist in four distinct conformational isomers.[18,22] As shown in Figure 6a, the N−N

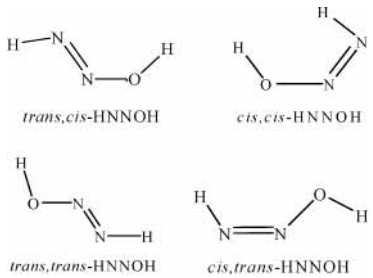

bond is essentially constant in all conformations while the N−O bond is somewhat more variable, ranging from 1.35 to 1.41 Å. Nonbonded repulsions between H atoms destabilize the *cis,cis* conformer by several kcal mol^{-1} with respect to the other conformations, while the *cis,trans* isomer is slightly preferred. H-transfer from H_2NNO initially produces the *trans,cis*-HNNOH conformer, which must isomerize into the *cis,trans* conformer preceding the second H-transfer. Two isomerization paths are possible depending on the sequence of distortions about the N−N and N−O bonds (Figure 6a). Isomerization about the N−O bond occurs by simple rotation with relatively little activation energy (11 kcal mol^{-1} from *trans,cis* to *trans,trans*, 4 kcal mol^{-1} from the less stable *cis,cis* to *cis,trans*). Conversion of the stereochemistry about the more double-bond-like N−N bond has larger activation energy and occurs by bending of the HNN fragment rather than rotation. The activation energies with respect to the more stable endpoint are approximately 35 kcal mol^{-1}, in good agreement with previous evaluations.[13,14,18,22] The rate-limiting barrier in either pathway is approximately the same, and the order of these distortions is irrelevant to the subsequent H transfer reaction.

HNOOH has more intriguing conformational variability arising from rotations about the N−O and O−O bonds and that has not been studied previously. Like HNNOH, planar, *trans,-cis*-HNOOH radical is the product of H-transfer from H_2NOO radical. However, none of the other planar conformations of HNOOH are minima within the conformational space, and scans over the entire conformation space reveal only two other stable rotational conformers (each existing as two isoenergetic stereoisomers). The principle isomers are shown in Figure 6b, along with the transition states that connect them. Unlike H_2NNO, conformational changes about the N−O and O−O bonds are concerted and produce significant changes in both bond lengths, with the N−O length decreasing and O−O increasing substantially. These large changes reflect unusually strong coupling between conformation and electronic structure that would be of interest for further study in there own right. From a reactivity perspective, the activation energies for all the distortions are small and all conformers are close in energy, the most stable one leading being at the entrance to the second 1,3 H-transfer.

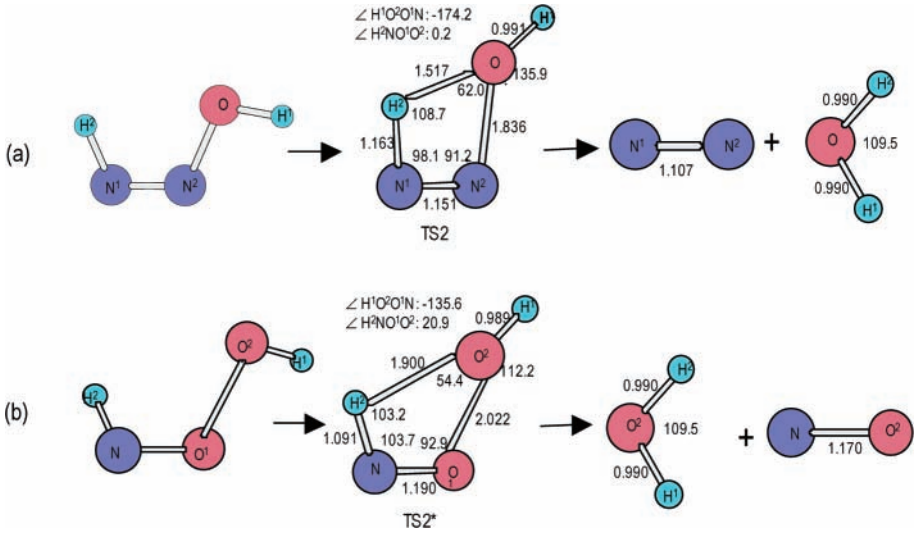

Figure 7. BLYP-calculated structures along (a) HNNOH → N_2 + H_2O and (b) HNOOH → NO + H_2O pathways.

HNXOH (X = N, O) → NX + H_2O 1,3 H-transfer. Once properly oriented, 1,3 H-transfers from HNXOH occur with the breaking of N−H and X−O bonds and formation of the second O−H bond. As with the first H-transfer reactions, the activation energies and transition state structures are similar along the two paths, and both reactions proceed through four-membered-ring transition states (labeled TS2 in Figure 1). Both reactions are exothermic and, as shown in Figure 7, have early transition states: the N−X bonds are shortened and X−O bonds are lengthened, but the H_2O product is highly distorted from its final structure. The calculated activation energies are 20 and 18 kcal mol^{-1} for X = N and O, respectively.

Discussion

The mechanistic origins of the NO selectivity that underpin thermal deNO_x are readily apparent from Figure 1. NH_3 itself is unreactive toward NO and O_2; rather, NH_3 is activated for reaction by removal of an H atom to produce NH_2 radicals. NH_2 radical forms a relatively strongly bond (40−50 kcal mol^{-1} from the best available calculations, Table 1) adduct with NO. Particularly favorable electronic interactions produce strong σ and π bonds (Figure 4) that are reflected in the molecular structure of H_2NNO. In contrast, NH_2 radical forms a very weakly bound adduct with O_2 (approximately 0 kcal mol^{-1} from the best available calculations, Table 3): O_2 has one more electron and less accessible 2π acceptor levels than NO, and H_2NOO radical has neither the strong σ nor π bonds of H_2-NNO. As seen in Figures 1 and 2, beyond the adduct formation step the potential energy surfaces for the two reactions are superficially quite similar. The paths to the thermodynamic products involve a sequence of H− transfer, isomerization, and decomposition steps, the most highly activated of which is the initial H_2NXO → HNXOH H-transfer. These steps compete with backward decomposition to reactants, and the balance between forward and backward steps controls the overall reaction rate. For strongly bound H_2NNO, the forward reaction steps are all at lower energy than the reaction entrance energy, and essentially all H_2NNO formed reacts forward to products in what is in effect a single elementary step.[44] In contrast, weakly bound H_2NOO radical is shifted upward in energy such that the forward reaction channels involve energy barriers greater than the energy to decompose back to reactants,[12] and only at high temperatures do any of the forward reaction channels occur at an appreciable rate.[20] *Remarkably, then, the difference in initial adduct stability alone accounts for the much different rates of the NH_2 + NO and NH_2 + O_2 reactions.* These two reactions are an example of the more general phenomenon of kinetics controlled by intermediate energetics.[58]

TABLE 5: Comparison of 298 K R−NO and R−O_2 Bond Strengths (kcal mol^{-1}; all values experimentally determined[60] unless otherwise noted)

	R−NO	R−O_2	Δ
H	47	49	−2
CH_3	40	33	7
i-C_3H_7	37	37	0
CF_3	43	37[a]	6
HO	49	7[b]	42
CH_3O	42	−4[c]	46
F	57	13	44
Cl	38	6	33
NH_2	48[d]/54[e]	0[e]/15[f]	∼40−50

[a] Calculated, ref 61. [b] Calculated, ref 62. [c] Calculated, ref 63. [d] Calculated, ref 18. [e] Calculated, ref 19. [f] Calculated, this work.

It is interesting to consider the generality of this difference in reactivity between NO and O_2. Table 5 compares the R−NO and R−O_2 bond dissociation energies for a number of common alkyl and heteroatomic free radicals R for which data are available. NO is found to readily bind to all the radicals within this sample set: bond strengths range from around 40 to less than 60 kcal mol^{-1}, with the strongest bonds tending to be to π donor radicals, such as NH_2 or OH radical. For practical purposes NO does not thermochemically discriminate within this set, and consistent with the behavior typical for free radical combination reactions, the corresponding R + NO high-pressure limiting rate constants are large—typically within an order of magnitude of the gas-kinetic limit.[59] O_2 presents an interesting contrast. Within the H and alkyl radical group, the R−O_2 and R−NO bond strengths are comparable and the difference between the two is uniformly small. Consistent with this, the R + O_2 reaction rate constants are comparable to those for R + NO, and thus these R exhibit little inherent selectivity in reactions with NO over O_2; i.e., neither CH_3 radical nor H radical will selectively combine with or reduce NO in the presence of O_2.

The heteroatom (halogen, O, and N)-centered radicals behave much differently. Here the R−O_2 bond energies are very small—so small that accurate experimental determination is difficult, and the most reliable estimates tend to come from first-principles calculations. While there are uncertainties in some of these

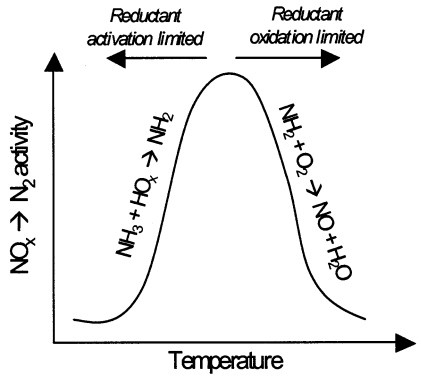

Figure 8. Schematic representation of NO_x conversion efficiency to N_2 as a function of temperature in thermal deNO_x.

R−O_2 bond energies, what is not uncertain is that the bonds are on the order of 40 kcal mol^{-1} weaker the R−NO ones. Because these are association reactions, the relative bond energies dominate the relative reaction rate constants, and the corresponding R + O_2 reactions are similarly much slower than the R + NO ones.[59] (Precise reaction rate comparisons are complicated by the existence of multiple reaction channels, large sensitivities to pressure, temperature, and diluent, and the limited availability of data for the slow R + O_2 reactions.) Thus, these heteroatomic radicals are not inherently selective for reactions with NO but rather are inherently selective *against* reaction with O_2. While we have only considered in detail the NH_2 radical case here, it is likely that the slow reactions of the other heteroatomic radicals with O_2 have similar explanations in terms of π repulsions and poor σ bonding. Any of these heteroatomic radicals will selectively combine with NO in the presence of O_2; NH_2 radical is particularly useful because it reacts with NO ultimately to produce N_2.

A complete description of thermal deNO_x chemistry would require inclusion of many more than just the NH_2 + NO and NH_2 + O_2 reactions described here, but the behavior of these two alone parallels and provides a useful framework for understanding general features of the heterogeneous selective catalytic reduction of NO_x. Like thermal deNO_x, the SCR of NO_x to N_2 is generally most effective in a relatively narrow temperature window for a given catalyst.[10] As shown schematically in Figure 8, the activity is limited at low temperature largely by the kinetics of NH_2 radical production, i.e., by conversion of the NH_3 reductant into an activated form via reactions with O_2.[9,38] At higher temperatures selectivity toward N_2 rapidly declines as the NH_2 + O_2 reactions become faster and the NH_2 + NO reaction becomes reversible, i.e., as H_2-NNO back decomposition competes more effectively with forward reaction. Similar features dominate NO_x SCR chemistry. Thus, one general function of an SCR catalyst is to facilitate reductant activation by reducing the intrinsic barriers to the activation process and/or by providing a site at which the activated reductant can bind and be stabilized. As with the thermal chemistry, activation can involve reaction with O_2 or O_2-derived species (such as NO_2); O_2 is well-known to promote NO_x SCR in many systems.[2,10] Of course the precise composition of the activated reductant will depend both on the catalyst and the introduced reductant; for NH_3 SCR over vanadia catalysts, adsorbed NH_2 is a plausible candidate, and in fact H_2NNO itself has been proposed as an intermediate in this catalytic chemistry.[22,64] For hydrocarbon-based SCR the range of plausible candidates is much greater, but substantial evidence exists for partially oxidized alkanes as key intermediates on base-metal catalysts.[65]

Once reductant is converted to an activated form, a second general requirement of a successful SCR system is inhibition of further reaction with O_2. Under practical conditions the oxidation reactions are thermodynamically favored, so the kinetic inhibitors to reaction must be substantial. As shown above, it is the amazing lack of reactivity of NH_2 radical toward O_2 that enables thermal deNO_x. Useful catalysts must exhibit the same property—the ability to activate reductants without catalyzing their complete oxidation. Hydrocarbon SCR using supported precious metal catalysts illustrate this tradeoff well: activity toward NO_x reduction requires temperatures great enough to initiate hydrocarbon activation, but activity rapidly degrades with temperature as complete hydrocarbon activation out competes NO reduction reactions.[66]

These concepts can be cast in terms of the following very simple mean field model of the competition between NO and O_2 for reductant on a catalyst surface. In this model, S represents a catalyst active site, S−NO and S−O_2 represent adsorbed NO and O_2, respectively (whether O_2 is treated molecularly or as dissociated into two S−O has no bearing on the qualitative conclusions), and R is a generic reductant that reacts with O_2 on the catalyst surface to form activated R*:

$$S + O_2 \leftrightarrow S{-}O_2 \tag{16}$$

$$S + NO \leftrightarrow S{-}NO \tag{17}$$

$$S{-}O_2 + R \leftrightarrow S{-}R^* \tag{18}$$

$$S{-}NO + S{-}R^* \rightarrow 2\,S + {}^1/_2\,N_2 + \text{oxidation products} \tag{19}$$

$$S{-}O_2 + S{-}R^* \rightarrow 2\,S + \text{oxidation products} \tag{20}$$

In reactions 19 and 20, R* is oxidized by NO or O_2 to produce (possibly different) gas-phase oxidation products. Assuming R* is formed on the surface irreversibly and is at steady state, the rate of NO conversion to N_2 is given by the following expression:

$$\frac{d[N_2]}{dt} = \frac{({}^1/_2)k_{18}\theta_{O_2}[R]}{1 + \left(\frac{k_{20}}{k_{19}}\right)\left(\frac{\theta_{O_2}}{\theta_{NO}}\right)} \tag{21}$$

where brackets indicate gas-phase concentrations and θ_X is the surface coverage of X. From the numerator of reaction 21, the NO conversion rate depends directly on the rate of activation of R to R*, which scales with the concentration of reductant and the surface coverage of O_2. The denominator captures the competition between adsorbed O_2 and NO for activated reductant. Rapid NO conversion is favored by a small rate constant ratio ($k_{20}/k_{19} \ll 1$) and low O_2 coverage relative to NO ($\theta_{O2}/\{\theta_{NO} \ll 1\}$). The O_2 coverage thus has competing influences on the NO conversion rate; further, the much greater concentration of O_2 than NO under practically interesting conditions ([O_2] ≫ [NO]) limits the extent to which NO conversion can be controlled through O_2 coverage alone. Thus, as in thermal deNO_x, the critical factor in promoting selective NO conversion is through k_{20}/k_{19}, i.e., through the relative rate constants for ultimate consumption of reductant by O_2 compared to NO. This rate constant ratio is on the order of 10^{-10} for thermal deNO_x, which gives a sense of the selectivity that must be achieved for effective NO_x SCR.

While this is clearly a highly idealized model, the general conclusions regarding NO and O_2 competition are robust and

reinforce conclusions derived from thermodynamic analysis of NO reduction.[67] The inherent competition between O_2 and NO is an important concept frequently overlooked in attempts to derive molecularly detailed mechanism of NO_x SCR chemistry. If the homogeneous, thermal deNO_x chemistry can serve as a guide, the absence of accessible reaction channels between activated reductant and O_2 is at least as fundamental to NO_x SCR as is the existence of reaction channels with NO, and is an important property both to be probed experimentally and to be captured in molecular-level models.

Conclusions

Any useful system for catalytically reducing NO_x in lean exhaust must have as its basis very high selectivity for reactions of reductant with NO_x over O_2, both to counterbalance the large thermodynamic preference for oxidation reactions and to overcome the large disparities in concentration between small amounts of NO_x and large amounts of background O_2. Within a limited range of conditions, this selectivity is achieved without catalysts in the thermal deNO_x process. NH_2 radicals generated in situ from NH_3 are many orders of magnitude more reactive toward NO than O_2. NH_2 radicals form a strong bond with NO to produce H_2NNO, which provides an entrance into rearrangement channels ultimately yielding the desired products N_2 and H_2O. What is unusual in this system, though, is not the fast rate of the NH_2 + NO reaction—in fact, this reaction proceeds at rates comparable to those of other radical + NO reactions. Rather, the key feature that underpins thermal deNO_x is the very slow reaction of NH_2 radical with O_2. The H_2NOO adduct is weakly bound, and fragmentation back to reactants competes very effectively with channels ultimately leading to NO and H_2O. This weak binding and slow reaction is characteristic of O_2 reactions with heteroatomic radicals, such as F, OH, or NH_2, but not of reactions with H or carbon-centered radicals. Its origins lie in π repulsions and weak σ bonding between O_2 and electron-rich radicals.

These observations offer a different perspective on the selective catalytic reduction of NO_x with NH_3 or hydrocarbons. Effective catalysts clearly must be able to bind and activate reductants and to maintain or enhance selectivity in reductant reactivity between NO and O_2. While mechanistic emphasis tends to be placed on understanding the reactivity of NO_x, the absence of reactivity with O_2 is at least as important to understand and enhance.

Acknowledgment. We gratefully acknowledge helpful discussions and comments from Chris Goralski, Ole John Nielsen, Steve Harris, Tim Wallington, Chris Wolverton, and Paul Schuck, as well as support from the Department of Energy under grant DE-F603-99ER14985 and from the National Center for Supercomputing Applications for computer resources on their SGI Origin cluster at project RTM (8141).

References and Notes

(1) Centi, G.; Perathoner, S. *Appl. Catal. A* **1995**, *132*, 179.
(2) Pârvelescu, V. I.; Grange, P.; Delmon, B. *Catal. Today* **1998**, *46*, 233.
(3) Tsekov, R.; Smirniotis, P. G. *J. Phys. Chem. B* **1998**, *102*, 9525.
(4) Shelef, M.; McCabe, R. W. *Catal. Today* **2000**, *62*, 35.
(5) Gandhi, H. S.; Graham, G. W.; McCabe, R. W. *J. Catal.* **2003**, *216*, 433.
(6) Bradford, M.; Grover, R.; Paul, P. *Chem. Eng. Prog.* **2002**, March, 42.
(7) Bradford, M.; Grover, R.; Paul, P. *Chem. Eng. Prog.* **2002**, April, 38.
(8) Miller, J. A.; Bowman, C. T. *Prog. Energy Combust. Sci.* **1989**, *15*, 287.
(9) Lyon, R. K. *Environ. Sci. Technol.* **1987**, *21*, 231.
(10) Busca, B.; Lietti, L.; Ramis, G.; Berti, F. *Appl Catal. B: Environ.* **1998**, *18*, 1.
(11) Lyon, R. K. *7th Diesel Engine Emissions Reduction (DEER) Workshop*, 2001; http://www.osti.gov/fcvt/deer2001/deer2001wkshp.html.
(12) Dean, A. M.; Bozzelli, J. W. In *Gas-Phase Combustion Chemistry*, Gardiner, W. C., Jr., Ed.; Springer: New York, 2000; pp 125−341.
(13) Wolf, M.; Yang, D. L.; Durant, J. L. *J. Phys. Chem. A* **1997**, *101*, 6243.
(14) Abou-Rachid, H.; Pouchan, C.; Chaillet, M. *Chem. Phys.* **1984**, *94*, 243.
(15) Vandooren, J.;, Bian, J.; Van Tiggelen, P. *J. Combust. Flame* **1994**, *98*, 402.
(16) Walch, S. P. *J. Chem. Phys.* **1993**, *99*, 5295.
(17) Harrison, J. A.; Maclagan, R. G. A.; Whyte, A. R. *J. Phys. Chem.* **1987**, *91*, 6683.
(18) Diau, E. W.-G.; Smith, S. C. *J. Chem. Phys.* **1997**, *106*, 9263.
(19) Sumathi, R.; Peyerimhoff, S. D. *J. Chem. Phys.* **1998**, *108*, 5510.
(20) Bozzelli, J. W.; Dean, A. M. *J. Phys. Chem.* **1989**, *93*, 1058.
(21) Marcy, P. T.; Heard, E. D.; Leone, R. S. *J. Phys. Chem. A* **2002**, *106*, 8249.
(22) Gilardoni, F.; Weber, J.; Baiker, A. *J. Phys. Chem. A* **1997**, *101*, 6069.
(23) Park, J.; Lin, M. C. *J. Phys. Chem. A* **1997**, *101*, 5.
(24) Roose, T. R.; Hanson, R. K.; Kruger, C. H. *Proc. 11th Int. Symp. Combust.* **1978**, 245.
(25) Park, J.; Lin, M. C. *J. Phys. Chem.* **1996**, *100*, 3317.
(26) Takeyama, T.; Miyama, H. *Bull. Chem. Soc. Jpn.* **1965**, *38*, 8.
(27) Michael, J. V.; Klemm, R. B.; Brobst, W. D.; Bosco, S. R.; Nava, D. F. *J. Phys. Chem.* **1985**, *89*, 3335.
(28) Fujii, N.; Miyama, H.; Koshi, M.; Asaba, T. *Symp. Proc. 18th Int. Symp. Combust.* **1981**, 873.
(29) Hack, W.; Horle, O.; Wagner, H. Gg. *J. Phys. Chem.* **1982**, *86*, 765.
(30) Baulch, D. L.; Cobos, C. J.; Cox, R. A. *J. Phys. Chem. Ref. Data* **1992**, *21*, 411.
(31) Tyndall, G. S.; Orlando, J. J.; Nickerson, K. E. *J. Geophys. Res.* **1991**, *96*, 20761.
(32) Sarkisov, O. M.; Cheskis, S. G.; Nadtochenko, V. A. *Arch. Combust.* **1984**, *4*, 111.
(33) Duan, X.; Page, M. *J. Mol. Struct. (THEOCHEM)* **1995**, *333*, 323.
(34) Miller, J. A.; Glarborg, P. *Int. J. Chem. Kinet.* **1999**, *31*, 757.
(35) Diau, E. W.; Yu, T.; Wagner, M. A. G.; Lin, M. C. *J. Phys. Chem.* **1994**, *98*, 4034.
(36) Dean, A. M.; Hardy, J. E.; Lyon, R. K. *Proc. 19th Int. Symp. Combust.* **1982**, 97.
(37) Hennig, G.; Klatt, M.; Spindler, B.; Wagner, H. Gg. *Bunsen. Ber. Phys. Chem.* **1995**, *99*, 651.
(38) Votsmeier, M.; Song, S.; Hanson, R. K.; Bowman, C. T. *J. Phys. Chem. A* **1999**, *103*, 1566.
(39) Yamasaki, K.; Watanabe, A.; Tanaka, A.; Sato, M.; Tokue, I. *J. Phys. Chem.* **2002**, *106*, 6563.
(40) Park, J.; Lin, M. C. *Proceedings of 4th International Conference, Technologies and Combustion for a Clean Environment;* Calouste Gulbenkian Foundation: Lisbon, Portugal, 1997; p 34.
(41) Lesclaux, R.; Khe, P. V.; Dezauzier, P.; Soulignac, J. C. *Chem. Phys. Lett.* **1975**, *4*, 493.
(42) Patrick, R.; Golden, D. M. *J. Phys. Chem.* **1984**, *88*, 491.
(43) Park, J.; Lin, M. C. *J. Phys. Chem.* **1999**, *103*, 8906.
(44) Miller, J. A.; Klippenstein, S. J. *J. Phys. Chem. A* **2000**, *104*, 2061.
(45) Atkinson, R.; Baulch, D. L.; Cox, R. A.; Hampson, R. F., Jr.; Kerr, J. A.; Rossi, M. J.; Troe, J. *J. Phys. Chem. Ref. Data* **1997**, *26*, 1329.
(46) DeMore, W. B.; Sander, S. P.; Golden, D. M.; Hampson, R. F.; Kurylo, M. J.; Howard, C. J.; Ravishankara, A. R.; Kolb, C. E.; Molina, M. J. "Chemical Kinetics and Photochemical Data for Use in Stratospheric Modeling"; Evaluation Number 12; *JPL Report 97-4*; Jet Propulsion Laboratory: Pasadena, CA, 1997.
(47) Silver, J. A.; Kolb, C. E. *J. Phys. Chem.* **1982**, *86*, 3240.
(48) Kaiser, E. W. *J. Phys. Chem.* **1993**, *97*, 11681.
(49) *NIST Chemistry Webbook*; National Institute of Standards and Technology; http://webbook.nist.org.
(50) Baerends, E. J.; Ellis, D. E.; Ros, P. *Chem. Phys.* **1973**, *41*, 1.
(51) Becke, A. D. *Phys. Rev. A* **1998**, *38*, 3098.
(52) Lee, C.; Yang, W.; Parr, R. G. *Phys. Rev. B* **1988**, *37*, 785.

(53) Miehlich, B.; Savin, A.; Stoll, H.; Preuss, H. *Chem. Phys. Lett.* **1989**, *157*, 200.
(54) Chase, M. W., Jr. NIST-JANAF Thermochemical Tables, 4th ed.; American Chemical Society (Washington, DC), and American Institute of Physics for the National Institue of Standards and Technology (Woodbury, NY; Monograph No. 9 of the Journal of Physical and Chemical Reference Data; 1998.
(55) Casewit C. J.; Goddard W. A. *J. Am. Chem. Soc.* **1982**, *104*, 3280.
(56) Huheey, J. A. *Inorganic Chemistry*, 3rd ed.; Harper & Row: New York, 1983.
(57) Melius, C. F.; Binkley, J. S. *Proc. 20th Int. Symp. Combust.* **1984**, 580.
(58) Donahue, N. M. *Chem. Rev.* **2003**, *103*, 4593.
(59) *NIST Chemical Kinetics Database*; National Institute of Standards and Technology: Washington, DC; http://kinetics.nist.gov.
(60) *CRC Handbook of Chemistry and Physics*, 84th ed.; CRC Press: Boca Raton, FL, 2003.
(61) Schneider, W. F.; Wallington, T. J. *J. Phys. Chem.* **1993**, *97*, 12783.
(62) Denis, P. A.; Kieninger, M.; Ventura, O. N.; Cachau, R. E.; Diercksen, G. H. F. *Chem. Phys. Lett.* **2002**, *365*, 440.
(63) Jungkamp, T. P. W.; Seinfeld, J. H. *Chem. Phys. Lett.* **1996**, *257*, 15.
(64) Anstrom, M.; Topsøe, N.-Y.; Dumesic, J. A. *J. Catal.* **2003**, *213*, 115.
(65) Tonkyn, R. G.; Barlow, S. E.; Hoard, J. W. *Appl. Catal. B: Environ.* **2003**, *40*, 207.
(66) Burch, R.; Coleman, M. D. *Catal. Today* **1995**, *26*, 185.
(67) Goralski, C. T., Jr.; Schneider, W. F. *Appl. Catal. B: Environ.* **2002**, *37*, 263.